



Original Paper

Gas Permeability Characteristics and Energy Evolution Laws of Gas-Bearing Coal under Multi-Level Stress Paths

Kang Peng,¹ Shaowei Shi,¹ Quanle Zou,^{1,3} Yongjiang Zhang,² and Guowen Tan²

Received 11 November 2019; accepted 10 February 2020

Published online: 20 February 2020

Gas permeability in coal characterizes the migration capacity of gas in coal, and it is an important parameter influencing the gas flow in a coal seam. Energy dissipation and energy release are important causes of rock mass failure. By utilizing a THM-2-type thermo-fluid–solid coupling test system for gas-bearing coal developed at Chongqing University, China, experimental research was conducted on raw coal samples from the Jinjia Coal Mine, Guizhou Province, China, under two different cyclic loading paths. The experimental results demonstrated that the overall change trends of permeability were consistent under the different loading and unloading paths and decreased exponentially with increasing stress. As the unloading level increased, the permeability hysteresis loops changed from sparsely to densely distributed and from spindle-shaped to crescent-shaped and ladder-shaped. The change laws of the upper and lower limits of permeability were closely related to the stress paths. The change trends of the lower limit of permeability under the two paths were consistent with that of the overall permeability and decreased exponentially with the increase in energy density. When the lower limit of unloading stress was constant, the upper limit of permeability gradually increased exponentially with increasing energy density, indicating that the gas permeability in the coal samples had strong hysteresis characteristics. The energy densities under the different paths nonlinearly increased with increasing stress; these relationships could be fitted by quadratic functions. The total input energy density showed the fastest rate of increase, followed by the elastic energy density, while the dissipated energy density had the slowest rate of increase, demonstrating that the energy evolution showed nonlinear characteristics. The experimental results were in good agreement with the evolution characteristics of the permeability of the stress loading and unloading zones in front of the working face. Understanding permeability from the perspectives of different stress loading and unloading paths and energy densities provides certain insights into the safe production and extraction of coalbed methane from coal mines.

KEY WORDS: Cyclic loading and unloading, Permeability, Energy density, Gas-bearing coal, Stress field.

INTRODUCTION

Coal resources that can be mined in from shallow strata in China are gradually being exhausted, so it is inevitable that resources will be mined from deeper depths (Li et al. 2016; Peng et al. 2019a, b, c, 2020; Liu et al. 2019a, b; Zou et al. 2016).

¹State Key Laboratory of Coal Mine Disaster Dynamics and Control, College of Resources and Environmental Science, Chongqing University, Chongqing 400044, China.

²Gas Prevention and Control Branch, Chongqing Research Institute, China Coal Technology Engineering Group, Chongqing 400037, China.

³To whom correspondence should be addressed; e-mail: quanle-zou2016@cqu.edu.com

With the increase in mining depth, mining of coal resources is bound to be affected by “three high and one disturbance (high in situ stress, high ground temperature and high osmotic pressure as well as strong mining disturbance),” which induces a series of mine disasters. Of them, coal and gas outbursts have not been fundamentally elucidated, posing a great threat to the safety of deep mining and the effective development of coalbed methane (CBM) (Lu et al. 2012; Li et al. 2015; Yuan 2016; Zou et al. 2019, 2020). The occurrence mechanisms of gas outbursts are very complicated, and the corresponding loss is considerable. Moreover, the threshold of its occurrence cannot be quantified (Xin et al. 2018), which brings great difficulties to the prevention and control of such events. In terms of the mechanisms of coal and gas outbursts, most scholars think that it is the result of the joint actions of the in situ stress, gas pressure and physical properties of the coal (Beamish and Crosdale 1998; Wold et al. 2008; Yang et al. 2019a, b). The occurrence of coal and gas outbursts is closely correlated with parameters such as the gas pressure, mining-induced stress, coal strength and permeability evolution. Although gas poses a great threat to the safe production of coal mines, it is currently an important energy source as energy becomes increasingly scarce. Therefore, the understanding of the gas infiltration mechanisms of coal and rock can directly affect mining safety and the effective management and utilization of gas. In summary, studying the infiltration characteristics of gas-bearing coal under different stress paths is of great significance for understanding the occurrence mechanisms of gas outbursts.

A coal mass is a special porous material, and its permeability is mainly determined by its structure. Coal is composed of void spaces and a matrix (Warren and Root 1963; Harpalani and Schraufnagel 1990), and the pores and fractures developed inside provide not only space for gas storage but also migration channels (Close 1993). Gas permeability is a key parameter for evaluating coal and gas outbursts and changes with other factors (Yin et al. 2013; Li et al. 2017; Zhao et al. 2018; Chao et al. 2019). The gas permeability and migration velocity of coal are affected by factors such as temperature and pressure (Connell 2009; Pan and Connell 2012; Perera et al. 2012). The evolution of permeability with temperature can be divided into four stages

(Teng and Wang 2016), i.e., thermal expansion, thermal volatilization, thermal fracturing and crack coalescence. Rutqvist et al. (2008) proposed that high temperatures can cause cracks and microcracks in rock to close. At medium and high temperatures (Morrow et al. 2001; Moore 2012), the gas permeability of coal and rock decreases with time (Polak et al. 2004). As the effective stress increases, the porosity and permeability of coal samples decrease exponentially (Durucan and Edwards 1986; McKee et al. 1987; Seidle et al. 1992; Levine 1996; Kelemen and Kwiatek 2009; Majewska et al. 2010; Czerw 2011; Li 2013).

At present, many scholars have conducted many studies and achieved many results on permeability (Palmer and Mansoori 1996; Clarkson and Bustin 1999; Siriwardane et al. 2009; Wang et al. 2011; Kumar et al. 2012; Kasani and Chalaturnyk 2017; Zou and Lin 2018; Yang et al. 2019a, b) and mechanical characteristics (Aziz and Wang 1999; George and Barakat 2001; Viète and Ranjith 2007; Masoudian et al. 2014; Xie et al. 2017; Wu et al. 2020) of gas-bearing coal. Experimental research on the gas permeability of coal under triaxial loading was carried out (Gentzis et al. 2007; Liu et al. 2019a, b; Wang et al. 2019a, b). The permeability of coal is influenced by the deformation characteristics and shear degree of the coal seam, and the gas permeability results of coal samples in different layers show an exponential relationship with the maximum, intermediate and minimum principal stresses as well as the effective stress. The influences of the intermediate principal stress on the minimum gas permeability of coal indicate a stress-sensitive zone. By comparing the evolution of gas permeability of gas-bearing coal under many different stress paths, Zhang et al. (2017) and Xin et al. (2018) found that permeability–strain curves under different stress paths can be divided into multiple stages. In addition, tests on the sensitivity of the gas permeability of coal to stress and porosity at five different depths demonstrated that with the increase in effective stress, the porosity and permeability of the coal samples decreased at each depth, obeying a negative exponential function (Zhang et al. 2019).

In addition to the above-mentioned studies, many scholars have also carried out a series of cyclic loading and unloading tests based on the actual environment of underground coal mining. Zhang and Zhang (2019) experimentally studied the stress–

permeability relationship of broken coal, rock and coal and rock sample combinations of various sizes under cyclic loading and unloading. They believed that the permeability stress sensitivity and permeability loss of the first loading and unloading are significantly greater than those of the subsequent loading and unloading cycles. Chu et al. (2019) conducted a triaxial cyclic loading test on coal samples and defined the permeability recovery rate to analyze the permeability observed in the triaxial cyclic loading–unloading test. Zou et al. (2019) experimentally determined the effective stress coefficient of coal during gas infiltration and studied the effect of effective stress and gas slip on coal permeability under cyclic loading conditions. Liu et al. (2019a, b) used a surface potential test system to study the characteristics and mechanism of the surface potential of gas-bearing coal under different loading modes (uniaxial compression, cyclic loading and gradient loading). They believed that the surface potential signal generated by coal during gas adsorption has a memory effect. This study provides theoretically meaningful practical results and reflects the microscopic process of coal fracturing. In addition to their research methods, Wang and Ma (2019), Mostafa (2019), Ghaitani (2019) and Wang et al. (2019a, b) proposed innovative theoretical derivation methods and research ideas that can be used to study the permeability characteristics of coal under different circulation paths and provided reference data. Through the various above-mentioned studies, a rigorous theoretical framework has been formed. However, the migration of gas in coal and rock and fracturing-induced failure of coal are very complex processes and can influence each other. For example, the fracturing and failure of coal can affect its gas permeability characteristics. Nevertheless, the failure of coal and rock materials is essentially driven by energy, and the energy characteristics are very important and effective for describing the mechanical performances of rock materials. Energy evolution includes energy input, storage, dissipation and release (Brady and Brown 1985; Mcsaveney and Davies 2009; Wasantha et al. 2014; Gong et al. 2019a, b). At present, the relationship between energy and the gas permeability of coal has not been fully studied. Therefore, research on the gas permeability of coal and rock from the perspective of energy can provide guidance for the infiltration mechanisms of gas in coal and rock and the prevention of coal and gas outbursts.

EXPERIMENTAL METHOD

Experimental Setup

In these experiments, the self-developed THM-2-type thermo-fluid–solid coupling test system of gas-bearing coal was used. This test system mainly includes four parts, i.e., a control system, a hydraulic system, a gas supply system and a power system. This equipment can be used to research experimentally the infiltration laws of gas in coal and rock and the deformation and failure of gas-bearing coal in the infiltration process under the coupling effects of different temperatures, in situ stresses and gas pressures. Table 1 shows the basic parameters of the device, and Figure 1 presents the test system. Each test was carried out according to the following steps:

1. Silica gel was uniformly smeared on the coal sample to prevent the leakage of gas from the coal wall. After the silica gel was completely dry, the sample was placed between the top and bottom of a pressure shaft in a triaxial chamber.
2. The coal sample was put onto a special heat-shrinkable tube for laboratory use, and a high-temperature blower was used to heat the tube so that the tube closely contacted the wall of the sample and the two ends of the pressure shaft.
3. Metal hoops were added to both ends of the pressure shaft to tighten the heat-shrinkable tube to prevent hydraulic oil from flowing into the tube. After that, an extensometer and the remaining parts of the triaxial flow meter were installed.
4. The oil was added into the chamber to limit the pressure. The preset confining pressure (2 MPa) and axial stress (2 MPa) were applied to simulate the conditions of isotropic in situ stress.
5. Methane gas was injected, and the test started after adsorption equilibrium.

Sample Preparation

The coal samples used in this experiment were mainly collected from a highly gassy mine—Jinjia Coal Mine, Liupanshui City, Guizhou Province,

Table 1. Basic parameters of the equipment

Specifications		
Dimension of specimen	50 × 100	mm
Maximum axial stress	1000	kN
Maximum confining pressure	10	MPa
Maximum gas pressure	6	MPa
Maximum axial displacement	60	mm
Maximum toroidal deformation	6	mm
Axial force control mode	Stress and displacement control	

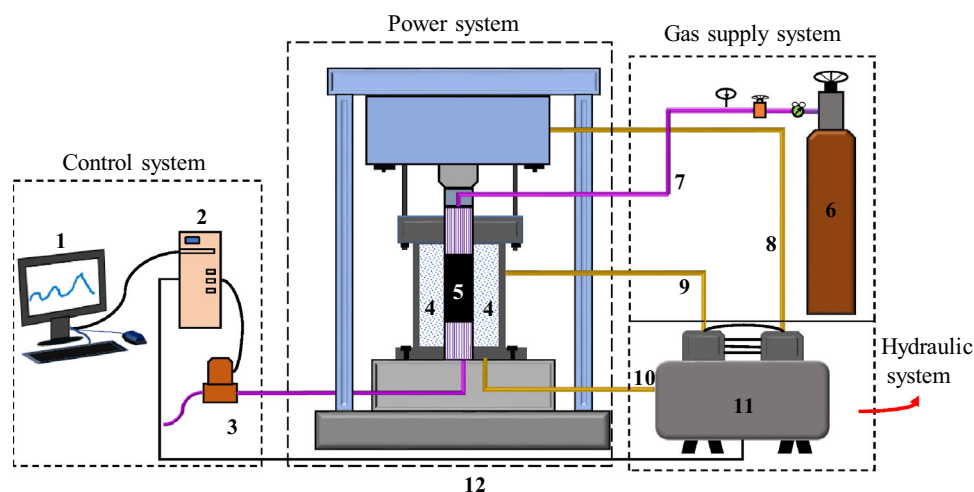


Figure 1. THM-2-type thermo-fluid-solid coupling test system of gas-bearing coal (1—monitor; 2—control system; 3—flow meter; 4—hydraulic oil; 5—sample; 6—gas cylinder; 7—gas pipe; 8, 9, 10—oil pipeline; 11—oil pump; 12—control circuit).

China. The coal was mainly found as powders and fragments, followed by lumps and scaly shapes, and its mechanical strength is low. The raw coal with a high calorific value was suitable for civil use and power generation. The obtained raw coal was processed and polished into cylindrical samples with dimensions of 50 mm × 100 mm to ensure that the parallelism and perpendicularity of the upper and lower surfaces of a sample met the relevant rock mechanics regulations. Figure 2 demonstrates the geographical location of the coal samples, and Table 2 presents proximate and elemental analysis results of the coal samples.

Experimental Program

The experiments on the gas permeability of gas-bearing coal were conducted under different cyclic loading and unloading paths. By taking methane as the experimental gas, the experiments were performed under an axial pressure of 1 MPa and a confining pressure of 2 MPa in the load control mode. When the axial stress was loaded to 2 MPa, the program control was selected to stabilize the pressure. In addition, by utilizing 1 MPa of methane gas, cyclic static loading and unloading in the axial direction were performed on the samples after adsorption equilibrium of the methane gas.

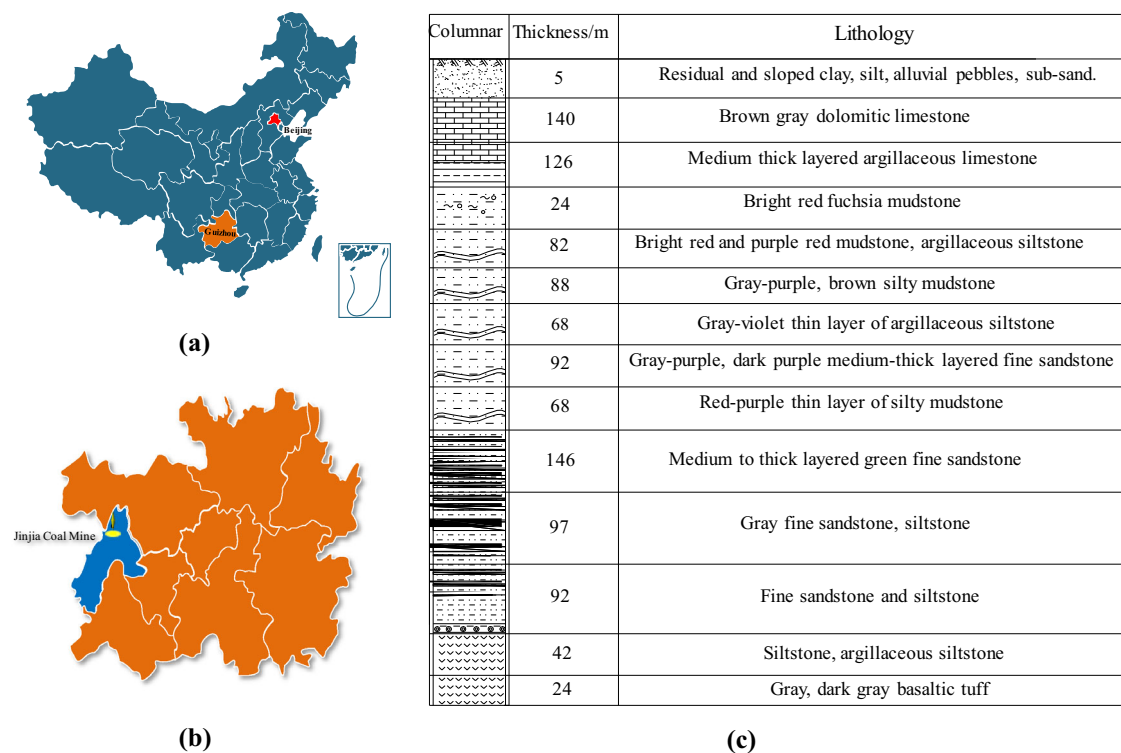


Figure 2. Geographical location of coal samples. (a) Location of Guizhou Province. (b) Location of the Jinjia Coal Mine. (c) Stratigraphic column.

Table 2. Proximate and elemental analyses

Industrial analysis			Total sulfur	Elemental analysis		
Moisture	Ash	Volatile matter	S_{td} (%)	Phosphorus	Hydrogen	Nitrogen
M_{ad} (%)	A_d (%)	V_{daf} (%)	1.01	p_d (%)	H_{daf} (%)	N_{daf} (%)
2.36	20.49	24.30		11.56	4.95	1.22

ad = Air-dried basis; d = dry basis; td = total dry basis; daf = dry ash free

Under stress path I, the lower limit of the unloading stress was maintained, while the upper limit of the loading stress was changed by increasing the amplitude of the stress level. In other words, after unloading to the hydrostatic pressure, the stress was increased to different upper limits (unloading level) at each time. The upper limit of the stress increased with the increase in the amplitude of the stress level. This could be expressed as follows: hydrostatic pressure (2 MPa) → 4 MPa → 2 MPa → 6 MPa → 2 MPa → 8 MPa → 2 MPa → 10 MPa → 2 MPa → 12 MPa → 2 MPa → 14 MPa. Each cycle was performed in the same manner, and 10

cycles were performed at each level. The test did not stop until the samples exhibited damage.

Under stress path II, the lower limits of the unloading stress and upper limits of the loading stress were both changed, while the increase in the amplitude of the stress level remained unchanged at 2 MPa. In other words, the lower limit of the unloading stress at the next level was the upper limit of the loading stress at the previous level, expressed as follows: hydrostatic pressure (2 MPa) → 4 MPa → 2 MPa → 6 MPa → 4 MPa → 8 MPa → 6 MPa → 10 MPa → 8 MPa → 12 MPa → 10 MPa → 14 MPa → 12 MPa. Each cycle was performed in the same manner, and each

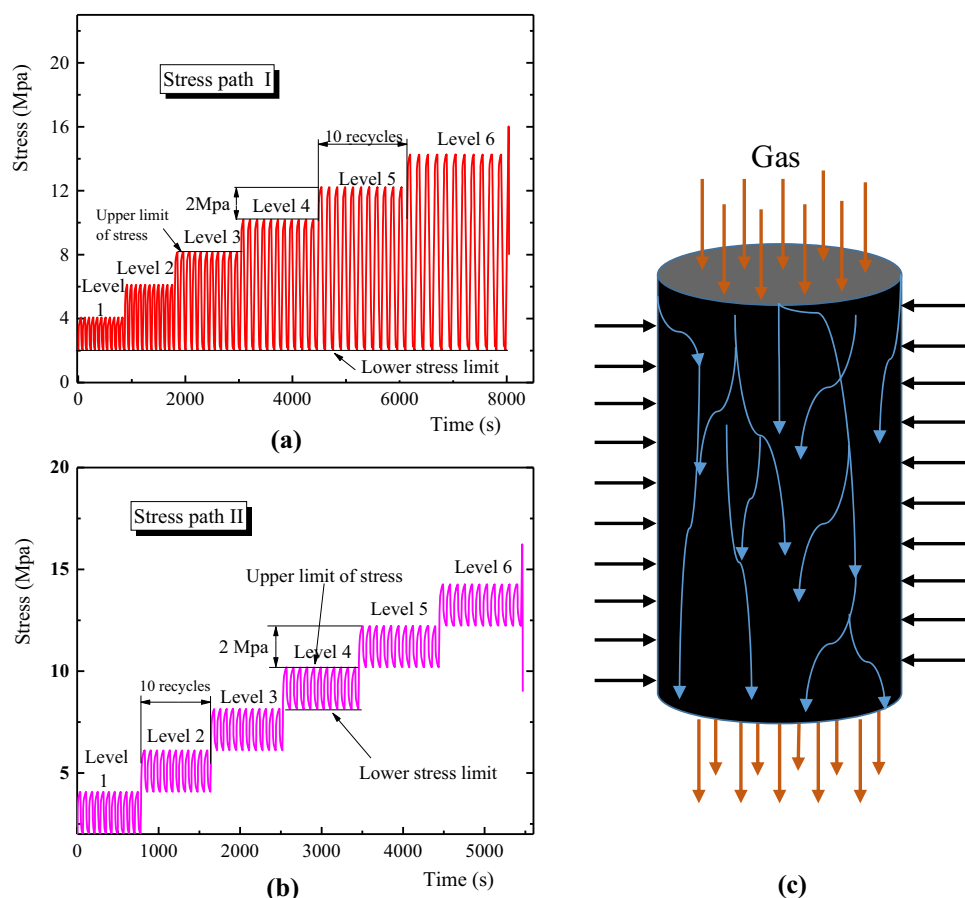


Figure 3. Diagrams of loading–unloading stress paths. **(a)** Stress path I. **(b)** Stress path II. **(c)** Flow model of gas inside a coal sample.

level included 10 cycles. The test did not stop until the samples exhibited damage. These two stress paths are shown in Figure 3.

Calculation Method of Energy Density

The process of rock deformation and failure is accompanied by energy dissipation and release (Gong et al. 2019a, b). Energy evolves throughout the process of rock deformation and failure: Energy is generally constantly input into coal and rock from the outside in the form of mechanical energy; part of this energy is stored in the rock in the form of elastic energy, while the other is dissipated, generating plastic and irreversible deformation. Studying rock failure from the perspective of energy can capture essential attributes of rock failure. This study used energy density as a reference value, and the real

energy was the product of the energy density and the actual volume of a sample. Assuming that there was no heat exchange between the sample and the external environment in the experimental process, according to the laws of conservation of energy and thermodynamics, the total energy density produced by work done by external forces could be expressed as follows (Xie et al. 2009).

$$U = U^e + U^d \quad (1)$$

where U , U^d and U^e represent the total energy density, the dissipated energy density and the elastic energy density, respectively.

Graphically, the area enclosed by the loading curve and abscissa is the total energy density, while the area enclosed by the unloading curve and abscissa is the elastic energy density. The dissipated energy density is the difference between the total

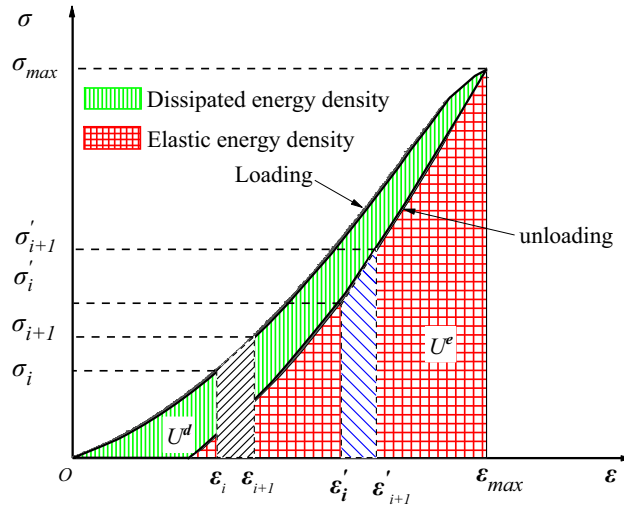


Figure 4. Schematic diagram for the calculation of energy density.

energy density and elastic energy density. Figure 4 presents a schematic diagram of the calculation of energy density, and the calculation method is shown as follows (Meng et al. 2016; Liu et al. 2019a, b; Peng et al. 2019a, b, c).

$$\begin{cases} U = \sum_{i=1}^n \frac{1}{2}(\sigma_i + \sigma_{i+1})(\varepsilon_i - \varepsilon_{i+1}) \\ U^e = \sum_{i=1}^m \frac{1}{2}(\sigma'_i + \sigma'_{i+1})(\varepsilon'_i - \varepsilon'_{i+1}) \end{cases} \quad (2)$$

$$U^d = U - U^e \quad (3)$$

where σ_i , σ_{i+1} , σ'_i and σ'_{i+1} indicate the stresses on the integral unit, ε_i , ε_{i+1} , ε'_i and ε'_{i+1} represent the strains on the integral unit, and σ_{max} and ε_{max} denote the stress and strain corresponding to the unloading level, respectively.

Principle underlying Calculation of Permeability

In the laboratory, the gas permeability of the samples can be measured by using three methods, the gas flow method, pulse method and quasi-static method (Wang et al. 2014). Supposing that the infiltration process of gas in coal and rock in the experiment was an isothermal process, the gas permeability of the samples was calculated according to the Darcy-Weisbach formula (Somerton et al. 1975; Jasinge et al. 2011; Wang et al. 2013).

$$K = \frac{2Q\mu p_a L}{A(P_1^2 - P_2^2)} \quad (4)$$

where K , μ , L , Q and A represent permeability (m^2), gas viscosity (Pa s), sample length (m), methane flow (m^3/s) and cross-sectional area (m^2) of the sample, respectively, and P_a ; P_1 ; and P_2 indicate the atmospheric pressure (Pa), pressure (Pa) at air inlet and pressure (Pa) at air outlet, respectively. In this experiment, because the outlet pipe led to the atmosphere, $P_a = P_2$. By substituting the experimental data into Formula (4), the gas permeability of the samples could be calculated.

RESULTS

Stress–Strain Relationships for Different Stress Paths

Figure 5 shows stress–strain curves under cyclic loading. It can be seen from the figure that although the stress–strain curves under the two different loading and unloading paths share certain similarities, they have considerable differences. Under the two stress paths, the loading and unloading stress–strain curves do not overlap, and each cyclic loading and unloading can produce a plastic hysteresis loop. Moreover, hysteresis loops at the same level do not overlap. This indicates that the coal samples generate elastic and plastic deformation in the cyclic

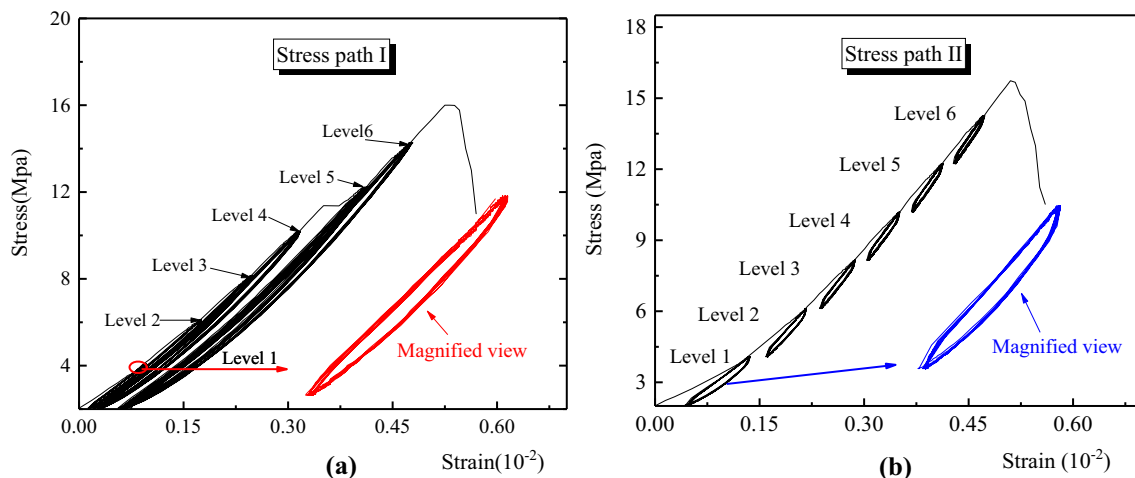


Figure 5. Two stress–strain curves. (a) Stress path I; (b) stress path II.

loading and unloading process and reflect that the coal samples are subjected to fatigue damage under the effects of cyclic loading (Peng et al. 2019a, b, c). Under the effects of cyclic loading, the elastic deformation of the coal samples completely recovers after unloading, while the plastic deformation that cannot completely recover is called irreversible deformation (Peng et al. 2019a, b, c), the magnitude of which is directly related to the damage degree of the coal samples. Under path I, with the increase in loading and unloading stress levels, the plastic hysteresis loops clearly enlarge. Under path II, plastic hysteresis loops at each stress level do not overlap. With the increase in the stress level, the elastic hysteresis loops show a decreasing trend. This suggests that the influences of the loading and unloading along path II on the coal are smaller than those along path I. In general, the stress–strain curves show the following characteristics (Hobbs 1964; Medhurst and Brown 1998; Wang et al. 2013). (1) The initial nonlinear part of the stress–strain curve is concave up, which results from the closure of the natural pores and fractures in the coal. (2) The linear-elastic range of the stress–strain curve is known as the elastic deformation stage, from which Young’s modulus can be determined in compression. (3) The final nonlinear part of the stress–strain curve caused by fracturing is called the fracture development stage. After entering into this stage, the development of microfracturing changes qualitatively, and the fractures continue to develop until the sample is completely damaged.

Loading and Unloading Elastic Modulus

Coal is a porous medium that is affected by the geologic environment during the formation process. Coal contains a large number of primary pores and microcracks, resulting in coal being a nonideal elastic material. When the coal body is subjected to external forces, the closure of the primary pores and the development of epigenetic damage will cause weak deformation of the coal rock. When these weak deformations have accumulated to a certain extent, some macroscale strength parameters can be realized. The elastic modulus is an important performance parameter of engineering materials and can be regarded as an index to measure the difficulty of the elastic deformation of materials. Taheri (2016) assessed the progressive failure of rocks by loading a tangential elastic modulus of 50% of the amplitude. Others also use the secant elastic modulus and other forms of the elastic modulus as analysis and evaluation indicators (Taheri and Tatsuoka 2015). However, the elastic modulus used in this article is different from what they proposed. To better show the change in the elastic modulus at each loading and unloading point, we divide the elastic modulus into a loading elastic modulus and an unloading elastic modulus, which are defined as the ratio of stress to strain when loaded to the unloading level (σ_{\max}) and when unloaded to the initial stress (σ_0). According to the experimental data, we obtain the loading and unloading elastic moduli of the gas-bearing coal under the two paths, as shown in Figure 6. Figure 6 shows that the load-

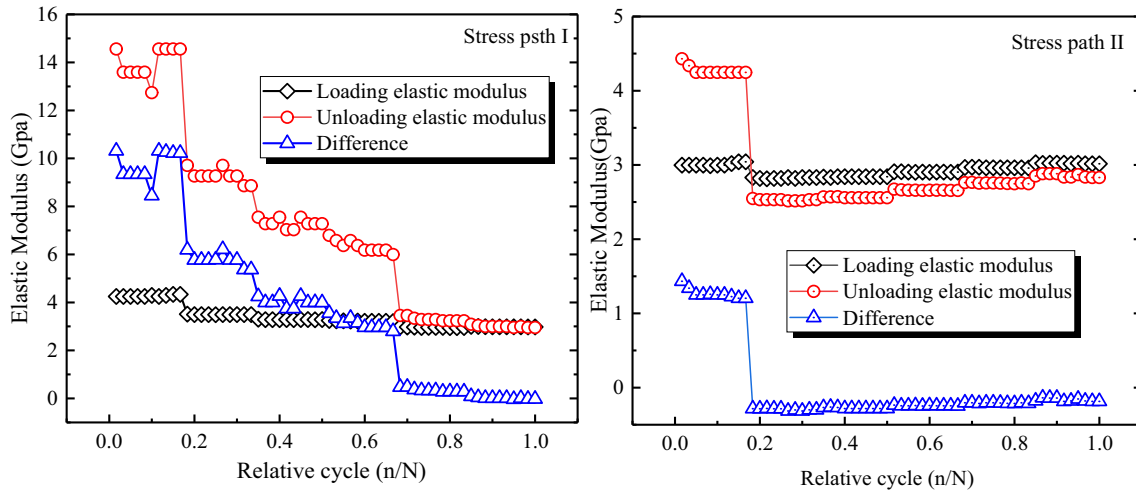


Figure 6. Elastic modulus of loading and unloading under two paths.

ing and unloading moduli of elasticity are the greatest during the initial cycle. As the upper limit of the stress gradient increases, the loading and unloading moduli of elasticity in path I show consistency, gradually decreasing as the number of cycles increases. As the stress increases and the cyclic gradient increases, the loading and unloading elastic moduli gradually approach each other and weaken. For path II, at the first stress level, the unloading elastic modulus is higher than the elastic loading modulus. As the stress gradient increases, the unloading elastic modulus becomes greater than the elastic loading modulus, and the laws of the loading and unloading elastic moduli change. They tend to be consistent, gradually increasing with the increase in the number of cycles and thus strengthening. Generally, the loading and unloading elastic moduli under the two stress paths approach each other with increasing stress gradient, that is, the loading and unloading elastic moduli become equal.

Irreversible Strain

Under normal circumstances, objects are deformed when subjected to external forces. When external forces are withdrawn, the deformation will gradually recover and exhibit elastic characteristics. However, due to the material characteristics of the object, including defects such as pores and cracks, the deformation cannot be completely restored to its original state after the external force is removed.

That is, part of the strain is reversible, and the irreversible part is called irreversible deformation, which exhibits certain plastic characteristics. The calculation method of irreversible deformation is shown in Figure 7. The irreversible strain of the rock for each of the two stress paths is the difference between the strain at the end of each cycle and the beginning of each cycle.

$$\Delta \epsilon_{irr}^{1(n)} = \epsilon_{1,60}^{1(n)} - \epsilon_{1,1}^{1(n)} \tag{5}$$

where $\Delta \epsilon_{irr}^{1(n)}$ and n refer to the increment in axial irreversible strain during a single loading and unloading cycle and the serial number of that cycle, respectively. Moreover, $\epsilon_{1,60}^{1(n)}$ represents the axial strain recorded at the last sampling point (that is, the 60th sampling point) of the n th cycle, and $\epsilon_{1,1}^{1(n)}$ is the axial strain recorded at the first sampling point in the n th cycle.

Therefore, through superposition, the axial irreversible strain was calculated as follows:

$$\epsilon_{irr}^1 = \sum_{n=1}^N \Delta_{irr}^1(n) \tag{6}$$

To illustrate more accurately the irreversible strain evolution, the relationship between the irreversible strain and the number of cycles is shown in Figure 8, and the relationship between the irreversible strain and stress is shown in Figure 9. Generally, the irreversible strain evolution laws under the two paths are the same. Figure 8 shows

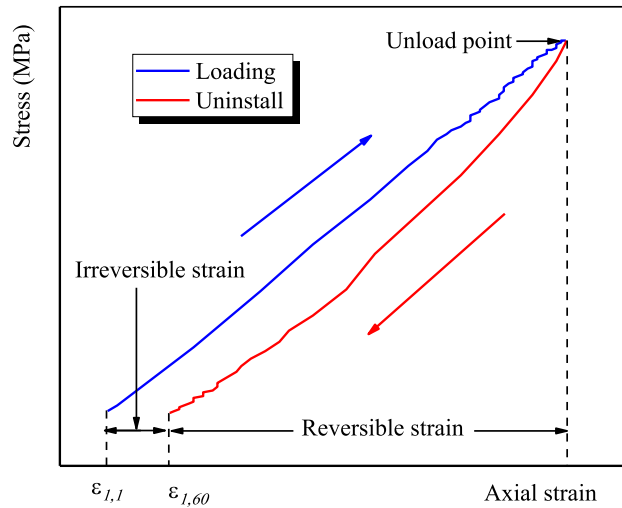


Figure 7. Schematic diagram of irreversible deformation calculation.

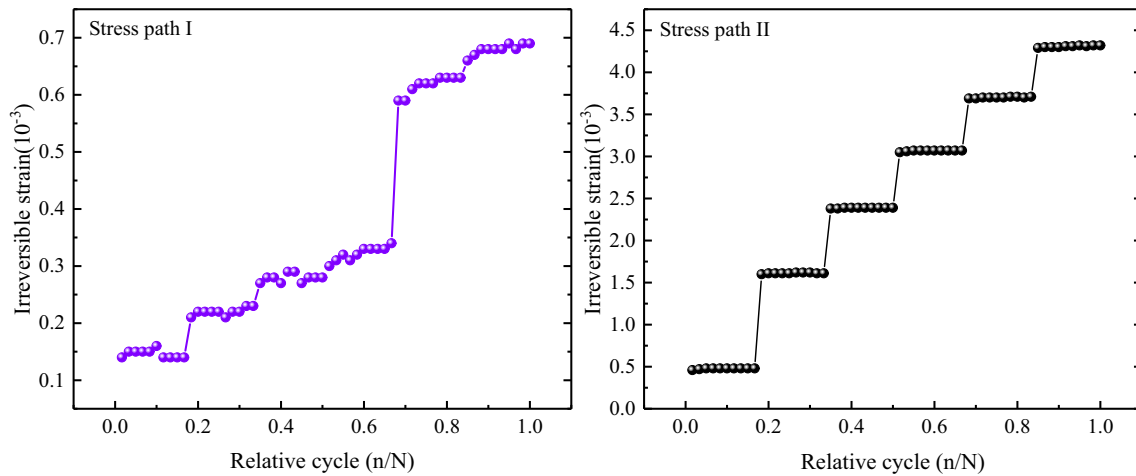


Figure 8. Relationship between irreversible strain and cyclic ratio.

that the irreversible strain increases as the number of cycles increases. At the same time, we also observed that for path I, the irreversible strain changed sharply between the fourth and fifth levels due to local damage to the coal sample. For path II, the irreversible strain shows a stepwise increase with increasing stress gradient and number of cycles. In addition, Figure 9 clearly shows that the irreversible strain increases at different speeds between the two paths, and the growth rate of path I is significantly greater than that of path II. This shows that the contribution of irreversible strain for path I is

greater and increases faster than that for path II. With the continuous accumulation of irreversible strain, macroscopic cracks eventually occur, and the specimen is destroyed.

Instantaneous Permeability

Gas migration in coal mass and coal failure is very complex processes, and fracturing and failure of coal and permeability characteristics of gas are important factors affecting coal and gas outbursts.

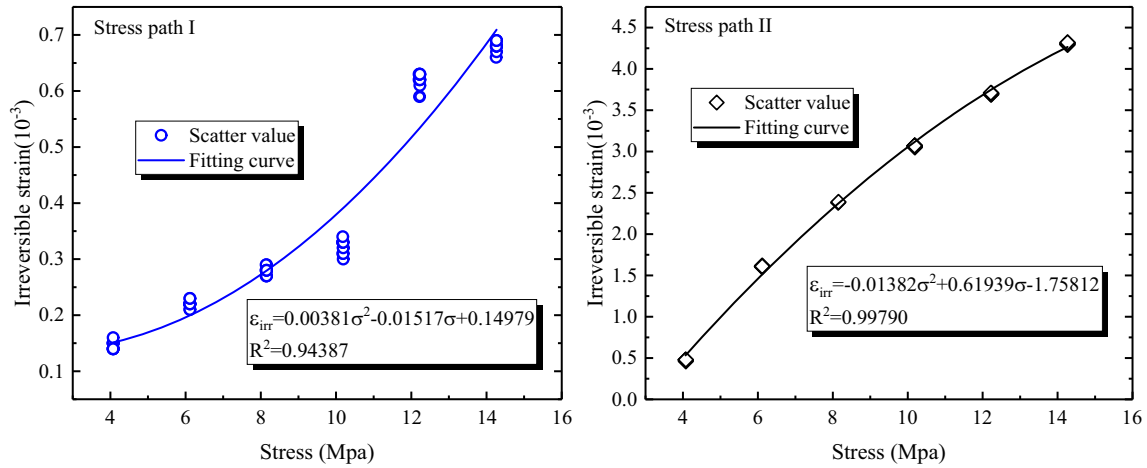


Figure 9. Relationship between irreversible strain and stress.

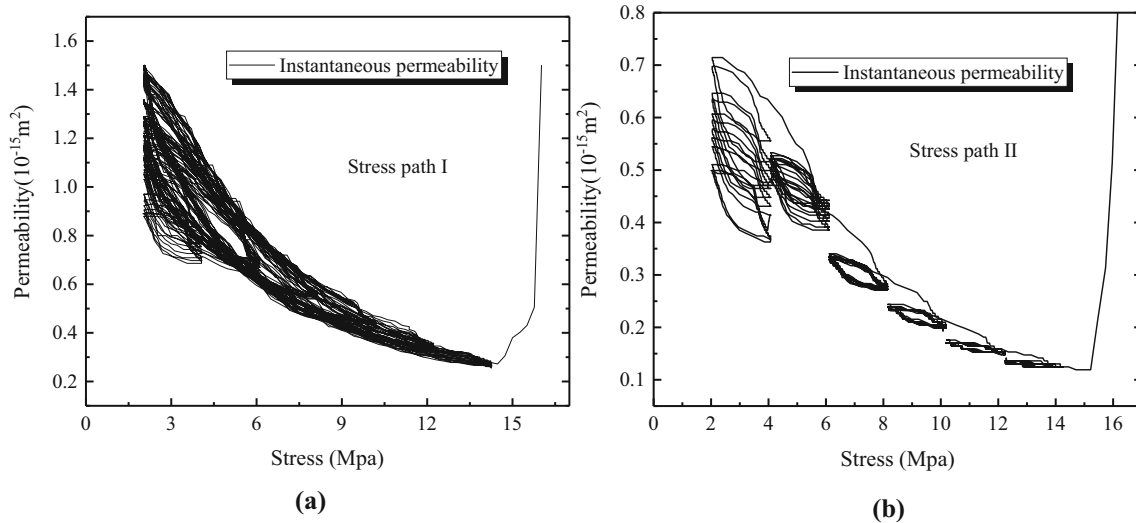


Figure 10. Transient permeability in two paths. (a) Relationship between instantaneous permeability and stress for path I. (b) Relationship between instantaneous permeability and stress for path II.

The flow channels of gas in coal are closely linked to the method of stress change. However, the deformation and failure of a rock mass is essentially the result of the combined action of energy dissipation and energy release. Energy dissipation mainly induces damage to the rock mass and degrades the material properties, while energy release is the internal cause of sudden failure of the rock mass. In the test process, the pores and fractures in the coal constantly change, causing the migration channels of the gas in the coal

mass to change. Figure 10b shows the relationship between the instantaneous permeability and stress for path II. The permeability of coal is very sensitive to stress because the cracks and pores of the coal body tend to close under the action of an external compressive force, so the permeability decreases as the axial stress increases. By comparing Figure 10a, b, it is not difficult to find that the permeability decreases gradually with the increase in the stress under the two different paths and has nonlinear characteristics.

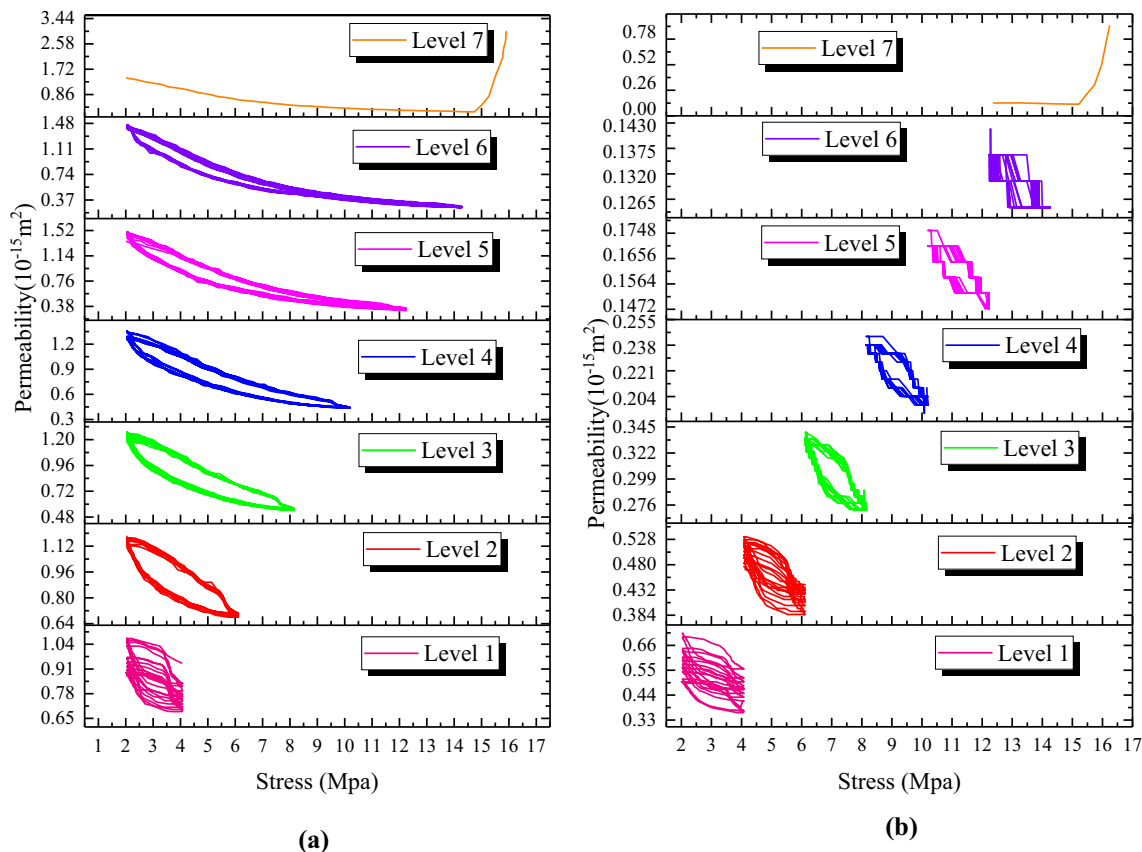


Figure 11. Relationship between permeability and stress. **(a)** Relationship between instantaneous permeability and stress at each level under path I. **(b)** The relationship between instantaneous permeability and stress at each level under path II.

DISCUSSIONS

Relationship Between Permeability and Stress

Figure 11a demonstrates the relationship among the cycles at each level under path I. The gas permeability of coal is sensitive to stress. Under the effects of an external compressive force, cracks and pores in the coal mass tend to close, so the permeability decreases with increasing axial stress. According to Figures 10a and 11a, at the same level, the permeability curves under loading and unloading do not overlap but do exhibit obvious hysteresis loops. In the 10 cycles at the first level, the permeability hysteresis loops are sparse and show a relatively plump spindle shape. With increasing stress level, the permeability hysteresis loops become denser, and the spindle shape gradually changes into a crescent shape during the 10 cycles at the same level.

Figure 11b demonstrates the relationship between the instantaneous permeability and stress among the cycles at each level under path II. Under path II, the overall permeability gradually decreases with increasing stress, and the hysteresis loops of the permeability gradually decrease with increasing stress level. As shown in Figure 11b, the cycles at the first level have the sparsest permeability hysteresis loops, and the second level exhibits the second-sparsest permeability hysteresis loops. The permeability hysteresis loops at the first two levels are clearly observable and have plump spindle shapes. From the third level, the permeability hysteresis loops tend to densify slightly. Similarly, the spindle shape becomes less obvious with increasing stress level, and the permeability curve under loading and unloading shows a stepped shape.

In Figure 11a, b, under paths I and II, the permeability hysteresis loops in the cycles at the first level are sparse. From the second stress level, per-

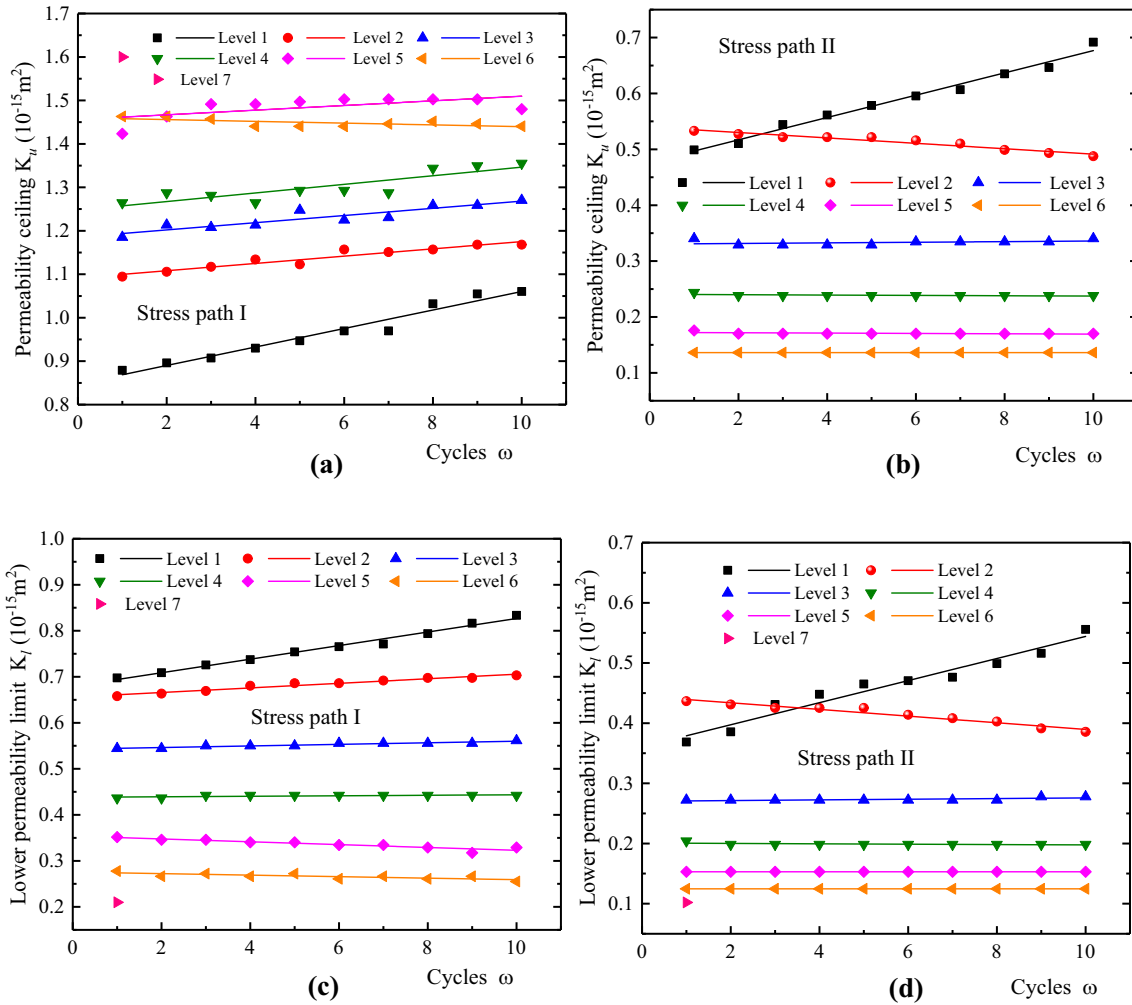


Figure 12. Curves of the upper and lower limits of permeability under the two stress paths. (a) The upper limit of the permeability under path I and (b) the upper limit of the permeability under path II; (c) the lower limit of the permeability under path I and (d) the lower limit of the permeability under path II.

meability hysteresis loops under path I gradually tend to densify, while those under path II still show obvious sparse characteristics but then gradually become dense.

Evolution Characteristics of Permeability

Figure 12 demonstrates the change laws of the upper and lower limits of permeability corresponding to each stress level under the two stress paths. As shown in Figure 12a, under path I, the upper limit of permeability presents four obvious stages: a rapid growth, stable growth, slow growth and slow decrease. Under path II in Figure 12b, the upper limit of permeability mainly exhibits three stages: a rapid

growth, slow decrease and stable stage. (There is no slow decrease stage as that under path I.) For the lower limit of permeability, the changes with stress path show differences in three stages, that is, a rapid increase, slow increase and stable stage under path I in Figure 12c and a rapid increase, slow decrease and stable stage under path II in Figure 12d. The change laws of the upper and lower limits of permeability under the two paths are different. Furthermore, it can be easily found that the change laws of the upper and lower limits of permeability are consistent under stress path II in Figure 12d. This indicates that the evolution laws of permeability are affected by the stress paths and that different loading and unloading paths exert different influences on permeability. Comparing the two stress paths, it is

found that during the unloading process, the stress of path I is completely released, while that of path II is not. Therefore, these two paths have different effects on fractures and pores. Moreover, compared with the loading and unloading paths with constantly increasing amplitudes at each stress level, the loading and unloading paths with increased amplitudes at each stress level have more obvious effects on permeability. The first stage in Figure 12 shows that the permeability increases with the number of cycles. There are two main reasons for this phenomenon. On the one hand, the test starts after the gas is fully adsorbed and balanced, and a large amount of gas is adsorbed by the coal sample. As the number of cycles increases, the adsorbed gas is released. On the other hand, the increase in the number of cycles causes some damage to the coal sample. However, in the initial stage, the latter has less influence on the increase in permeability. Table 3 shows the fitting expressions of permeability with the number of cyclic loadings at each unloading stress level. R^2 equals 0.27273, which shows that the lower limit of permeability is not a fixed value, that is, the permeability fluctuates. When R^2 equals 1, the lower limit of permeability is a fixed value and does not change with the increase in the number of cycles.

Relationship Between Energy Density and Stress

The failure of rock materials is essentially driven by energy, so it is very important and effective to describe rock materials from the perspective of energy. Under the effects of external loads, the energy change during rock deformation and failure is a dynamic process, including energy input, storage, dissipation and release. Before the failure of rock materials, energy can be stored in the form of elastic energy, and the total energy input from the outside environment can be divided into two parts, i.e., elastic energy and dissipated energy. The former generates elastic strain, while the latter produces plastic deformation. According to the calculation method for energy density in section “[Calculation Method of Energy Density](#),” energy densities can be obtained under the two paths. Figures 13 and 14 show the energy evolution laws of the coal samples under paths I and II, respectively. It can be seen from the figures that the energy density increases with stress and shows obvious nonlinear growth characteristics. The relationship between energy density and stress obeys a quadratic relation, as

displayed in Table 4. With the increase in stress, the total input energy density increases the fastest, followed by the elastic energy density, while the dissipated energy density increases the slowest. R^2 is used to describe the degree of fit of the curves in Table 4. R^2 refers to how well the regression line fits the observations (Mostafa 2019). Table 4 shows that the maximum and minimum R^2 of the relationship curve under path I is 0.99997 and 0.98284, respectively, while those are 0.99243 and 0.98640 under path II. This suggests that the quadratic function can accurately express the above nonlinear growth trend and that the energy evolution mechanism of coal and rock has very typical nonlinear characteristics in the process of loading and unloading. In addition, in accordance with the fitting curves in Figures 13 and 14, the elastic energy density is always similar to the total input energy density, while the dissipated energy density is greatly different from the elastic energy density and the total input energy density. This finding indicates that the elastic energy density stored in coal and rock is relatively high, while the dissipated energy density is low.

Evolution of Permeability with Energy Density

Energy and permeability characteristics can be combined to analyze the evolution laws of permeability from the perspective of energy, which is of profound significance to prevent disasters, such as coal and gas outbursts. In accordance with stress levels, permeability can be classified into the upper limit of permeability K_u and the lower limit of permeability K_l . The former is defined as the permeability while unloading to the lowest stress value, while the latter refers to the permeability when loading to the unloading level. The lower limit of the stress level corresponds to the upper limit of permeability, while the upper limit of the stress level corresponds to the lower limit of permeability. Because the total input energy density is the total of the elastic energy density and dissipated energy density, this study only discusses the relationships between permeability and elastic energy density and between permeability and dissipated energy density. As displayed in Figure 3, the lower limit of the stress level corresponds to the upper limit of permeability, while the upper limit of stress corresponds to the lower limit of permeability. Figure 15 shows the changes in the upper limits of permeability with elastic and dissipated energy densities under the two stress

Table 3. The fitting relationship between the permeability and the number of cyclic loadings at each unloading stress level

Stress path	Level	$K_u - \omega$ (10^{-15})	R^2	$K_1 - \omega$ (10^{-15})	R^2
Path I	1	$K_u = 0.02127\omega + 0.84754$	$R^2 = 0.96364$	$K_1 = 0.01474\omega + 0.67932$	$R^2 = 0.98725$
	2	$K_u = 0.00839\omega + 1.09137$	$R^2 = 0.91860$	$K_1 = 0.04980\omega + 0.65588$	$R^2 = 0.95808$
	3	$K_u = 0.00828\omega + 1.18550$	$R^2 = 0.85067$	$K_1 = 0.01720\omega + 0.54285$	$R^2 = 0.90188$
	4	$K_u = 0.00990\omega + 1.24750$	$R^2 = 0.75615$	$K_1 = 0.00055\omega + 0.43814$	$R^2 = 0.48485$
	5	$K_u = 0.00536\omega + 1.45617$	$R^2 = 0.40970$	$K_1 = -0.00309\omega + 0.35854$	$R^2 = 0.86428$
	6	$K_u = -0.00203\omega + 1.49950$	$R^2 = 0.43550$	$K_1 = -0.00165\omega + 0.27558$	$R^2 = 0.58182$
Path II	1	$K_u = 0.01997\omega + 0.47707$	$R^2 = 0.98310$	$K_1 = 0.01835\omega + 0.36064$	$R^2 = 0.95545$
	2	$K_u = -0.00485\omega + 0.53983$	$R^2 = 0.93404$	$K_1 = -0.00553\omega + 0.44494$	$R^2 = 0.94751$
	3	$K_u = 0.00005\omega + 0.33040$	$R^2 = 0.13853$	$K_1 = 0.00005\omega + 0.27092$	$R^2 = 0.48485$
	4	$K_u = -0.00003\omega + 0.24043$	$R^2 = 0.27273$	$K_1 = -0.00003\omega + 0.20073$	$R^2 = 0.27273$
	5	$K_u = -0.00003\omega + 0.17238$	$R^2 = 0.18182$	$K_1 = 0.15310$	$R^2 = 1$
	6	$K_u = 0.13609$	$R^2 = 1$	$K_1 = 0.12475$	$R^2 = 1$

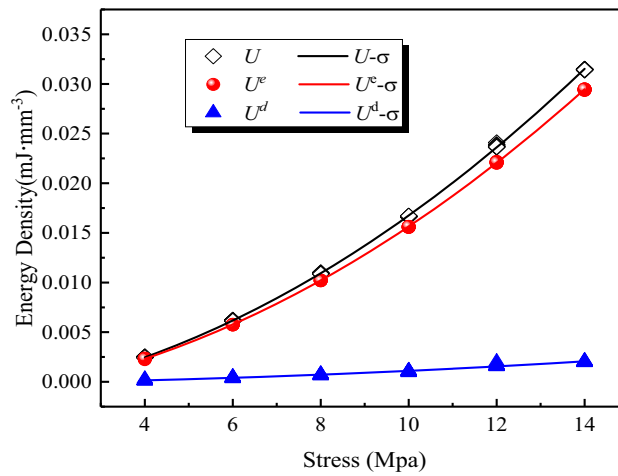


Figure 13. Energy evolution of the coal samples under path I.

paths. Figure 15 shows that the change laws of the upper limit of permeability are largely different under different loading and unloading paths. Under path I, as shown in Figure 15a, c, the change laws of the upper limit of permeability with elastic energy density and dissipated energy density are the same. The upper limit of permeability nonlinearly increases with the energy density, showing a positive correlation; this relationship can be accurately fitted by a quadratic function. The upper limit of permeability under path II has a change trend that diverges from that under path I. Figure 15b, d shows that the upper limit of permeability nonlinearly decreases with increasing elastic and dissipated energy densities. The negative correlation between the upper limit of permeability and energy density can be fitted with a quadratic function.

Figure 16 presents the evolution process of the upper limit of permeability under the effects of the two stress paths. The upper limit of the stress level corresponds to the lower limit of permeability. In Figure 16, the lower limit of permeability nonlinearly decreases with increasing elastic and dissipated energy densities. As the stress level increases, the elastic and dissipated energy densities increase nonlinearly (Peng et al. 2019a, b, c). Based on the scatter plots of the permeability under the two stress paths, the lower limit of permeability fluctuates greatly in the initial stage and shows great discreteness among the 10 cycles at each level. As the stress increases, the data in the scatter plots of permeability gradually stabilize and become dense, approaching a certain point. With a constant increase in stress, the data in the permeability scatter

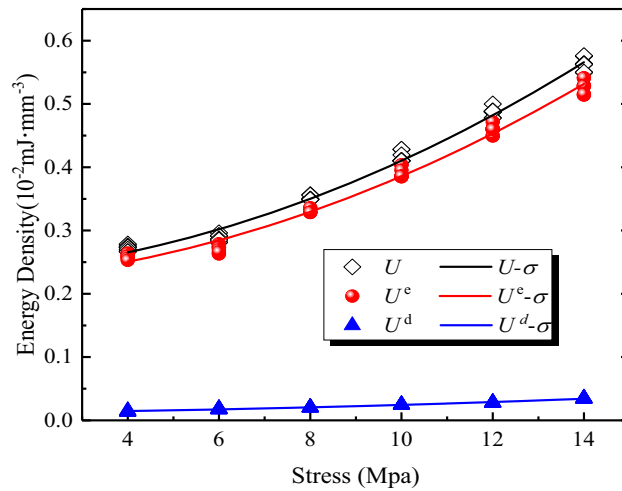


Figure 14. Energy evolution of the coal samples under path II.

Table 4. Fitting relationship between energy density and stress

Stress path	Abscissa	Ordinate	Fitting expression	Degree of fit
I	Stress (σ)	Total input energy density U	$U = 1.31591 \times 10^{-4}\sigma^2 + 5.36518 \times 10^{-4}\sigma - 0.00178$	$R^2 = 0.999$
	Stress (σ)	Elastic energy density U^e	$U^e = 1.23676 \times 10^{-4}\sigma^2 + 5.36518 \times 10^{-4}\sigma - 0.00160$	$R^2 = 0.999$
	Stress (σ)	Dissipated energy density U^d	$U^d = 7.941481 \times 10^{-6}\sigma^2 + 4.90906 \times 10^{-5}\sigma - 0.00017$	$R^2 = 0.983$
II	Stress (σ)	Total input energy density U	$U = 0.14800 \times 10^{-4}\sigma^2 + 0.34000 \times 10^{-4}\sigma + 0.002282$	$R^2 = 0.992$
	Stress (σ)	Elastic energy density U^e	$U^e = 0.14000 \times 10^{-4}\sigma^2 + 0.2920 \times 10^{-4}\sigma + 0.0021669$	$R^2 = 0.991$
	Stress (σ)	Dissipated energy density U^d	$U^d = 0.08131 \times 10^{-4}\sigma^2 + 0.047849 \times 10^{-4}\sigma + 0.00012$	$R^2 = 0.986$

plots become discrete, which corresponds to the information in section “[Relationship between Permeability and Stress](#)”. Figure 14 shows that the evolution of energy has nonlinear characteristics. The energy density increases with increasing stress. The increase in stress results in a decrease in permeability. The effect of energy and stress on permeability is consistent. Because the energy density and stress increase simultaneously, they both affect the permeability by controlling changes in the fractures and pores. Table 5 shows the fitting relationship between permeability and energy density.

Infiltration Mechanisms

The migration law of gas in a coal seam is an important research topic for elucidating the mechanical mechanisms of coal and gas outbursts and provides an important basis for studying the highly efficient extraction and utilization of CBM. In

underground mining activities, factors such as mining disturbance can result in stress redistribution in coal and rock, and the new stress field is known as the mining-induced stress field (Qi et al. 2009). Changes in mining-induced stress can lead to the fracturing and failure of coal, which is an essential cause of the changes in permeability. To better couple the stress field with the gas infiltration field, it is assumed that the development of the mining-induced stress field is affected by the coal and rock properties, mining depth, mining method and roadway layout. Furthermore, it is supposed that the mining-induced stress field shows variability, dynamics, predictability and controllability. According to the relationship between permeability and stress, the mining-induced stress field can be coupled with the infiltration field, as shown in Figure 17, thus establishing their spatiotemporal evolution. In accordance with the advancing direction of coal mining, the stress field can be divided into four parts, namely, an unloading zone, a loading zone, a

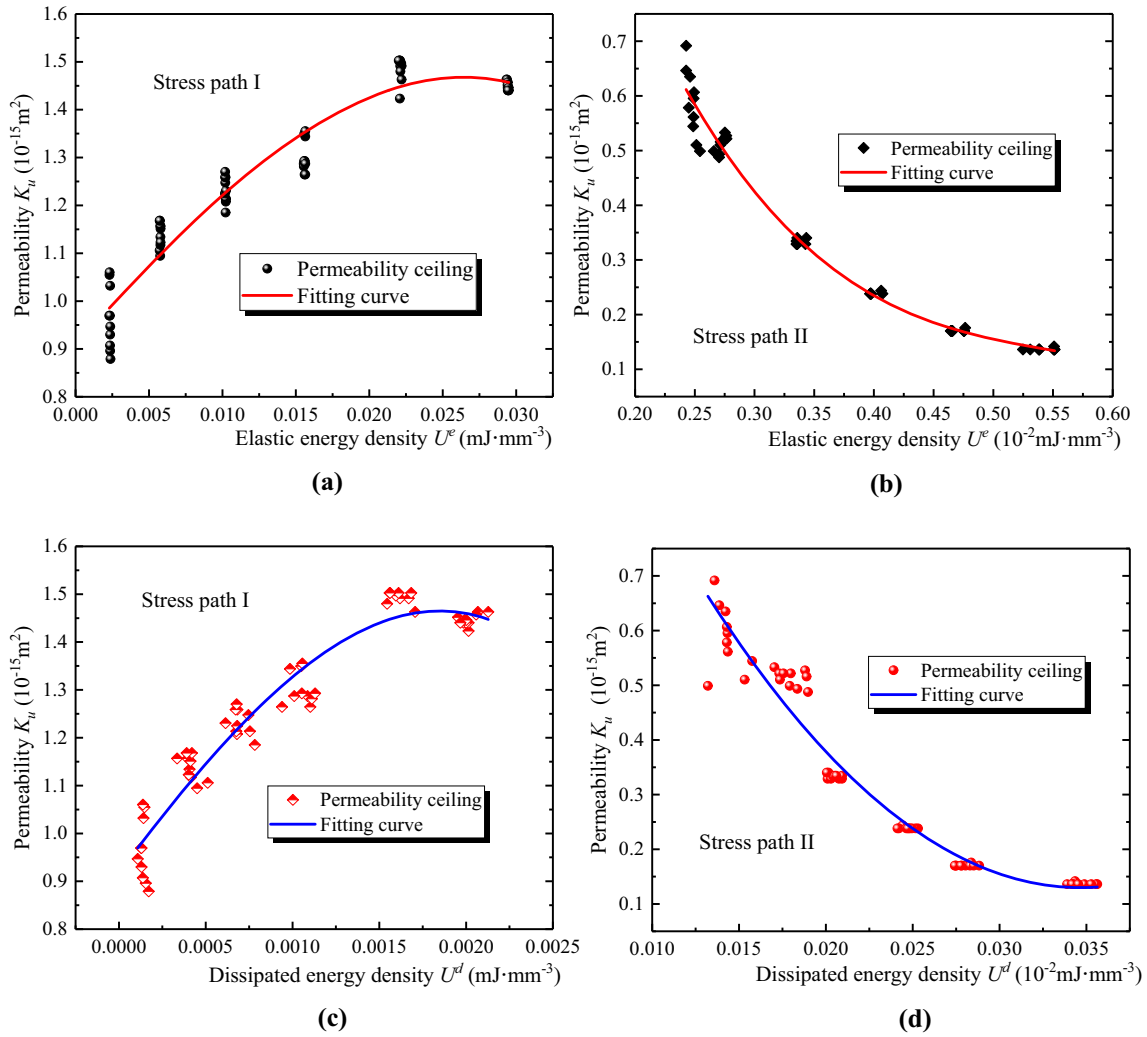


Figure 15. Relationship between the upper limit of permeability and energy density. **(a)** The relationship between K_U and U^e under stress path I. **(b)** The relationship between K_U and U^e under stress path II. **(c)** The relationship between K_U and U^d under stress path I. **(d)** The relationship between K_U and U^d under stress path II.

transition zone and an in situ stress zone. Similarly, based on the stress field, the infiltration field can be divided into four zones, namely, a sharp increase zone, a reduction zone, a transition zone and a primary infiltration zone. In the mining process, the gas migration direction is shown as the gas flow direction in Figure 17. In the loading and unloading zones, the permeability changes considerably. In the unloading zone, due to the influences of stress release and mining disturbance, more and larger cracks form in the coal mass, gradually forming macrocracks. Moreover, these changes cause the diameter of gas migration channels and the permeability to increase. The change law of gas permeability is consistent with that of the upper limit of

permeability in Figure 15. In the loading zone, the stress on the coal mass increases, and the original natural cracks and pores are compacted under the effects of high stress. Furthermore, the diameters of gas migration channel gradually decrease and close. Thus, the permeability decreases. The change law of gas permeability is similar to that of the lower limit of permeability in Figure 15. The transition between the unloading zone and the loading zone represents the boundary point and the maximum value on the stress arch, where the minimum permeability in the coal and rock occurs, corresponding to the lowest permeability in Figure 10a, b. The gasses on either side of this critical boundary flow in opposite directions tend to flow toward low-pressure areas. In

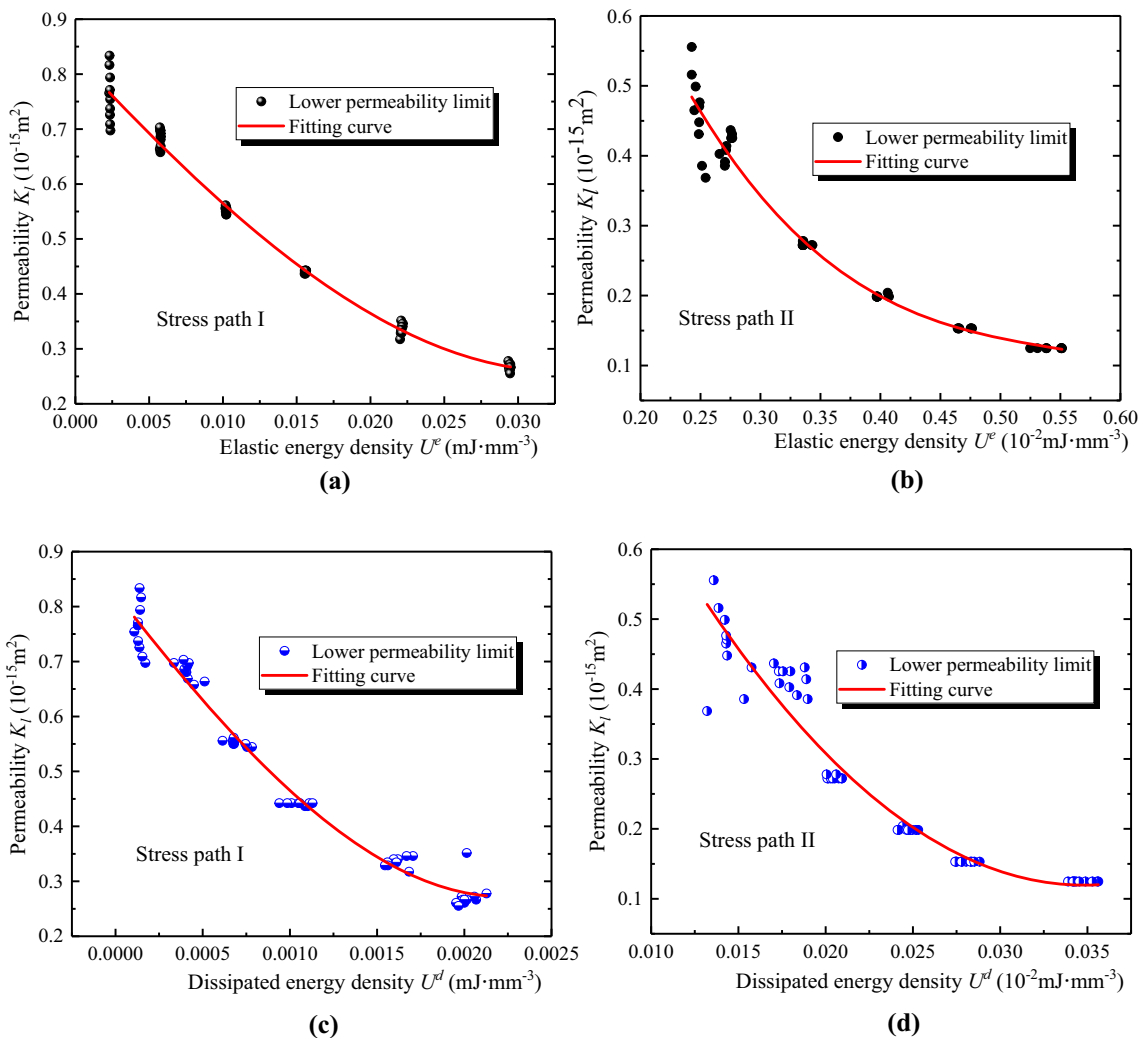


Figure 16. Relationship between the lower limit of permeability and energy density. **(a)** The relationship between K_L and U^e under stress path I. **(b)** The relationship between K_L and U^e under stress path II. **(c)** The relationship between K_L and U^d under stress path I. **(d)** The relationship between K_L and U^d under stress path II.

the transition zone and the in situ stress zone, the gas flow direction gradually becomes chaotic. In conclusion, the migration laws of gas under unloading in gas-bearing coal are closely correlated with permeability, while changes in abundant pressure have a large influence on permeability.

CONCLUSIONS

By utilizing the THM-2-type thermo-fluid-solid coupling test system of gas-bearing coal developed at Chongqing University, this study performed an experimental study on gas permeability characteristics in coal under two different loading and

unloading paths. A spatiotemporal evolution model coupling the stress field and gas infiltration field was built. From the perspective of energy, the gas permeability characteristics of the coal were quantitatively analyzed, and the evolution relationships of the upper and lower limits of permeability in the coal samples with energy density were characterized under the two stress paths. Through this research, the following conclusions were made.

1. Under the effects of high stress, the natural cracks and pores in the coal were constantly compacted, and the diameters of the gas migration channels were reduced, so the permeability decreased. Under unloading,

Table 5. Relationship between permeability and energy density

Stress path	Abscissa	Ordinate	Fitting expression	Degree of fit
I	K_u	Elastic energy density U^e	$K_u = -7.42964 \times 10^{-13}(U^e)^2 + 4.13546 \times 10^{-14}U^e + 8.88175 \times 10^{-16}$	$R^2 = 0.933$
	K_l	Elastic energy density U^e	$K_l = 4.34743 \times 10^{-13}(U^e)^2 - 3.23847 \times 10^{-14}U^e + 8.4186 \times 10^{-16}$	$R^2 = 0.987$
	K_u	Dissipated energy density U^d	$K_u = -1.44526 \times 10^{-10}(U^d)^2 + 5.69022 \times 10^{-13}U^d + 9.02635 \times 10^{-16}$	$R^2 = 0.932$
	K_l	Dissipated energy density U^d	$K_l = 9.03101 \times 10^{-13}(U^d)^2 - 4.58159 \times 10^{-13}U^d + 8.33242 \times 10^{-16}$	$R^2 = 0.979$
II	K_u	Elastic energy density U^e	$K_u = 5.65679 \times 10^{-11}(U^e)^2 - 5.97363 \times 10^{-13}U^e + 1.71809 \times 10^{-15}$	$R^2 = 0.981$
	K_l	Elastic energy density U^e	$K_l = 4.29392 \times 10^{-11}(U^e)^2 - 4.52844 \times 10^{-13}U^e + 1.3225 \times 10^{-15}$	$R^2 = 0.969$
	K_u	Dissipated energy density U^d	$K_u = 1.1583 \times 10^{-8}(U^d)^2 - 0.80288 \times 10^{-12}U^d + 1.152122 \times 10^{-15}$	$R^2 = 0.947$
	K_l	Dissipated energy density U^d	$K_l = 8.62271 \times 10^{-9}(U^d)^2 - 5.99977 \times 10^{-12}U^d + 1.16322 \times 10^{-15}$	$R^2 = 0.931$

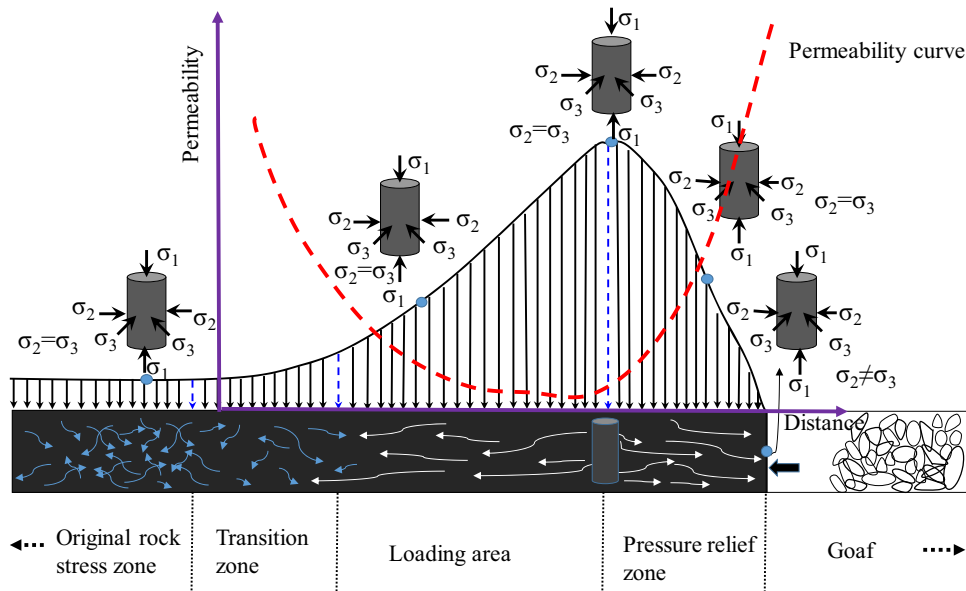


Figure 17. The model of the force of the coal mass and the permeability change curve in front of the coal mining face.

the fractures and pores in the coal expanded and the pore diameter increased, causing permeability to increase. The overall change trends of permeability were consistent under the different loading and unloading paths, and the permeability decreased exponentially with increasing stress. The permeability hysteresis loops changed from sparsely to densely distributed and from a spindle shape to a crescent shape and a ladder shape with the increase in unloading level. With the in-

crease in stress level, the spindle shape became less obvious.

2. The upper and lower limits of permeability under the two loading and unloading paths were fitted with the elastic and dissipated energy densities. The change laws of the upper and lower limits of permeability were closely related to the stress paths, and the change trends of the lower limits of permeability under the two paths were consistent with that of the overall permeability: With

the increase in energy density, the lower limits of permeability decreased in the form of an exponential function. When the lower limit of the unloading stress remained unchanged, the upper limits of permeability increased in the form of an exponential function with increasing energy density. This indicated that the coal had strong hysteresis characteristics.

3. By conducting the experiments on the coal samples under different loading and unloading paths, the total input energy density, elastic energy density and dissipated energy density all nonlinearly increased with the increase in stress and could be accurately fitted with a quadratic function. The total input energy density increased the fastest, followed by the elastic energy density, while the slowest increase was found in the dissipated energy density; that is, the energy evolution showed nonlinear characteristics.
4. The model coupling the stress field with the gas infiltration field could favorably describe the gas infiltration laws in front of the working face, and the variation in the stress arch was a key factor affecting permeability. In addition, the stress field was divided into four zones, namely, the unloading zone, the loading zone, the transition zone and the in situ stress zone. Corresponding to the stress field, the infiltration zone was divided into four zones, namely, the sharp increase zone, the reduction zone, the transition zone and the primary infiltration zone. Therefore, mastering the change laws of mining-induced stress could help to elucidate the corresponding gas infiltration characteristics. Particularly, under high-intensity mining and disturbance, gas infiltration changes completely. In the actual mining process in the coal mine, the behaviors of underground pressures should always be considered to ensure mining safety and prevent coal and gas outbursts.

ACKNOWLEDGMENTS

This work was funded by the State Key Research Development Program of China

(2017YFC0804206), Graduate Scientific Research and Innovation Foundation of Chongqing, China (Grant No. CYS19069), National Natural Science Foundation of China (51974043, 51774058 and 51704046), Chongqing Basic Research and Frontier Exploration Project (cstc2018jcyjA3320), and Special Fund Project for Scientific and Technological Innovation and Entrepreneurship of Tiandi Science & Technology Co., Ltd (2018-TD-MS076 and 2018-TD-QN059), which are gratefully acknowledged. The authors also thank the editor and anonymous reviewers very much for their valuable advices.

REFERENCES

- Aziz, N. I., & Wang, M. L. (1999). The effect of sorbed gas on the strength of coal—an experimental study. *Geotechnical and Geological Engineering*, 17, 387–402.
- Beamish, B. B., & Crosdale, P. J. (1998). Instantaneous outbursts in underground coal mines: an overview and association with coal type. *International Journal of Coal Geology*, 35, 27–55.
- Brady, B. H. G., & Brown, E. T. (1985). *Rock mechanics for underground mining*. Crows Nest: Allen & Unwin.
- Chao, J. K., Yu, M. G., Chu, T. X., Han, X. F., Teng, F., & Li, P. (2019). Evolution of broken coal permeability under the condition of stress, temperature, moisture content, and pore pressure. *Rock Mechanics and Rock Engineering*, 52, 2803–2814.
- Chu, Y. P., Sun, H. T., & Zhang, D. M. (2019). Experimental study on evolution in the characteristics of permeability, deformation, and energy of coal containing gas under triaxial cyclic loading–unloading. *Energy Science and Engineering*, (5).
- Clarkson, C. R., & Bustin, R. M. (1999). The effect of pore structure and gas pressure upon the transport properties of coal: a laboratory and modeling study. 1. *Isotherms and pore volume distributions*. *Fuel*, 78, 1333–1344.
- Close, J. C. (1993). Natural fracture in coal. *Studies in geology. Hydrocarbons from coal*, 38, 119–132.
- Connell, L. D. (2009). Coupled flow and geomechanical processes during gas production from coal seams. *International Journal of Coal Geology*, 79(1–2), 18–28.
- Czerw, K. (2011). Methane and carbon dioxide sorption/desorption on bituminous coal—experiments on cuboidal sample cut from the primal coal lump. *International Journal of Coal Geology*, 85, 72–79.
- Durucan, S., & Edwards, J. S. (1986). The effect of stress and fracturing on permeability of coal. *Min. Sci. Technol*, 3, 205–216.
- Gentzis, T., Deisman, N., & Chalaturnyk, R. J. (2007). Geomechanical properties and permeability of coal from the foothills and mountain regions of western Canada. *International Journal of Coal Geology*, 69, 153–164.
- George, J. D. S., & Barakat, M. A. (2001). The change in effective stress associated with shrinkage from gas desorption in coal. *International Journal of Coal Geology*, 45, 105–113.
- Ghaitani, M. M. (2019). Dynamic displacement calculation in beams structures considering the effect of nanoparticles as reinforcement phase. *International Journal of Hydromechanics*, 2(3), 237–246.

- Gong, F. Q., Yan, J. Y., Luo, S., & Li, X. B. (2019b). Investigation on the linear energy storage and dissipation laws of rock materials under uniaxial compression. *Rock Mechanics and Rock Engineering*, 52(12), 4237–4255.
- Gong, F. Q., Yan, J., Li, X. B., & Luo, S. (2019a). A peak-strength strain energy storage index for rock burst proneness of rock materials. *International Journal of Rock Mechanics and Mining Sciences*, 117, 76–89.
- Harpalani, S., & Schraufnagel, R. (1990). Shrinkage of coal matrix with release of gas and its impact on permeability of coal. *Fuel*, 69, 551–556.
- Hobbs, D. W. (1964). The strength and the stress-strain characteristics of coal in triaxial compression. *The Journal of Geology*, 72(2), 214–231.
- Jasinge, D., Ranjith, P. G., & Choi, S. K. (2011). Effects of effective stress changes on permeability of latrobe valley brown coal. *Fuel*, 90(3), 1292–1300.
- Kasani, H. A., & Chalaturnyk, R. J. (2017). Influence of high pressure and temperature on the mechanical behavior and permeability of a fractured coal. *Energies*, 10(7), 854.
- Kelemen, S. R., & Kwiatek, L. M. (2009). Physical properties of selected block argonne premium bituminous coal related to CO₂, CH₄, and N₂ adsorption. *International Journal of Coal Geology*, 77, 2–9.
- Kumar, H., Elsworth, D., Liu, J., Pone, D., & Mathews, J. P. (2012). Optimizing enhanced coalbed methane recovery for unhindered production and CO₂ injectivity. *International Journal of Greenhouse Gas Control*, 11(6), 86–97.
- Levine, J. R. (1996). Model study of the influence of matrix shrinkage on absolute permeability of coal bed reservoirs. *Coalbed Methane and Coal Geology*, 109, 197–212.
- Li, B. (2013). *Seepage characteristics of loaded coal containing gas and its application*. Beijing: China University of Mining and Technology.
- Li, X., Yan, X., & Kang, Y. (2017). Effect of temperature on permeability of gas adsorbed coal at triaxial stress conditions. *Journal of Geophysics & Engineering*, 15(2), 386.
- Li, X. L., Li, Z. H., Wang, E. Y., Feng, J. J., Chen, L., Li, N., & Kong, X. G. (2016). Extraction of microseismic waveforms characteristics prior to rock burst using Hilbert–Huang transform. *Measurement*, S0263224116302019.
- Li, Z. H., Wang, E. Y., Ou, J. C., & Liu, Z. T. (2015). Hazard evaluation of coal and gas outbursts in a coal-mine roadway based on logistic regression model. *International Journal of Rock Mechanics and Mining Sciences*, 80, 185–195.
- Liu, J. J., Gao, J. L., Zhang, X. B., Jia, G. N., & Wang, D. (2019a). Experimental study of the seepage characteristics of loaded coal under true triaxial conditions. *Rock Mechanics and Rock Engineering*, 52, 2815–2833.
- Liu, S. M., Li, X. L., Wang, D. K., Wang, D. K., Wu, M. Y., Yin, G. Z., et al. (2019b). Mechanical and acoustic emission characteristics of coal at temperature impact. *Natural Resources Research*. <https://doi.org/10.1007/s11053-019-09562-w>.
- Lu, C. P., Dou, L. M., Liu, H., Liu, H. S., Liu, B., & Du, B. B. (2012). Case study on microseismic effect of coal and gas outburst process. *International Journal of Rock Mechanics and Mining Sciences*, 53, 101–110.
- Majewska, Z., Majewski, S., & Zietek, J. (2010). Swelling of coal induced by cyclic sorption/desorption of gas: experimental observations indicating changes in coal structure due to sorption of CO₂ and CH₄. *International Journal of Coal Geology*, 83, 475–483.
- Masoudian, M. S., Airey, D. W., & Zein, El A. (2014). Experimental investigations on the effect of CO₂ on mechanics of coal. *International Journal of Coal Geology*, 12–23, s128–s129.
- McKee, C. R., Bumb, A. C., & Koenig, R. A. (1987). Stress-dependent permeability and porosity of coal and other geologic formations. In *International coalbed methane symposium*, SPE-12858-PA.
- Mcsaveney, M. J., & Davies, T. R. (2009). Surface energy is not one of the energy losses in rock comminution. *Engineering Geology*, 109(1–2), 109–113.
- Medhurst, T. P., & Brown, E. T. (1998). A study of the mechanical behaviour of coal for pillar design. *International Journal of Rock Mechanics and Mining Sciences*, 35(8), 1087–1105.
- Meng, Q. B., Zhang, M., & Han, L. (2016). Effects of acoustic emission and energy evolution of rock specimens under the uniaxial cyclic loading and unloading compression. *Rock Mechanics and Rock Engineering*, 49, 3873–3886.
- Moore, T. A. (2012). Coalbed methane: A review. *International Journal of Coal Geology*, 101, 36–81.
- Morrow, C. A., Moore, D. E., & Lockner, D. A. (2001). Permeability reduction in granite under hydrothermal conditions. *Journal of Geophysical Research: Solid Earth*, 106(B12), 30551–30560.
- Mostafa, S. M. (2019). Imputing missing values using cumulative linear regression. *CAAI Transactions on Intelligence Technology*, 4(3), 182–200.
- Palmer, I., & Mansoori, J. (1996). How permeability depends on stress and pore pressure in coalbeds: A new model. *SPE Reservoir Evaluation & Engineering*, 1, 539–544.
- Pan, Z., & Connell, L. C. (2012). Modelling permeability for coal reservoirs: A review of analytical models and testing data. *International Journal of Coal Geology*, 92, 1–44.
- Peng, K., Liu, Z. P., Zou, Q. L., Zhang, Z. Y., & Zhou, J. Q. (2019a). Static and dynamic mechanical properties of granite from various burial depths. *Rock Mechanics and Rock Engineering*, 1–22.
- Peng, K., Zhou, J. Q., Zou, Q. L., & Song, X. (2020). Effect of loading frequency on the deformation behaviours of sandstones subjected to cyclic loads and its underlying mechanism. *International Journal of Fatigue*, 131, 105349.
- Peng, K., Zhou, J. Q., Zou, Q. L., & Yan, F. Z. (2019b). Deformation characteristics of sandstones during cyclic loading and unloading with varying lower limits of stress under different confining pressures. *International Journal of Fatigue*, 127, 82–100.
- Peng, K., Zhou, J. Q., Zou, Q. L., Zhang, J., & Wu, F. (2019c). Effects of stress lower limit during cyclic loading and unloading on deformation characteristics of sandstones. *Construction and Building Materials*, 217, 202–215.
- Perera, M. S. A., Ranjith, P. G., Choi, S. K., & Airey, D. (2012). Investigation of temperature effect on permeability of naturally fractured black coal for carbon dioxide movement: an experimental and numerical study. *Fuel*, 94, 596–605.
- Polak, A., Yasuhara, H., & Elsworth, D. (2004). The evolution of permeability in natural fractures the competing roles of pressure solution and free-face dissolution. *Elsevier Geo-Engineering Book Series*, 2, 721–726.
- Qi, Q. X., Li, H. Y., Wang, Y. G., Deng, Z. G., Lan, H., Peng, Y. W., et al. (2009). Theory and test research on permeability of coal and rock body influenced by mining. *Journal of Coal Science and Engineering (China)*, 15(2), 143–147.
- Rutqvist, J., Freifeld, B., Min, K.-B., Elsworth, D., & Tsang, Y. (2008). Analysis of thermally induced changes in fractured rock permeability during 8 years of heating and cooling at the Yucca Mountain Drift Scale Test. *International Journal of Rock Mechanics and Mining Sciences*, 45(8), 1373–1389.
- Seidle, J. P., Jeanson, M. W., & Erickson, D. J. (1992). Application of matchstick geometry to stress dependent permeability in coals. *SPE Rocky Mountain Regional Meeting*, SPE-24361-MS.
- Siriwardane, H., Haljasmaa, I., Mclendon, R., Irdi, G., Soong, Y., & Bromhal, G. (2009). Influence of carbon dioxide on coal permeability determined by pressure transient methods. *International Journal of Coal Geology*, 77, 109–118.

- Somerton, W. H., Söylemezoglu, I. M., & Dudley, R. C. (1975). Effect of stress on permeability of coal. *International Journal of Rock Mechanics and Mining Science & Geomechanics Abstracts*, 12(5–6), 129–145.
- Taheri, A. (2016). Experimental study on degradation of mechanical properties of sandstone under different cyclic loadings. *Geotechnical Testing Journal*, 39(4), 20150231.
- Taheri, A., & Tatsuoka, F. (2015). Small- and large-strain behaviour of a cement-treated soil during various loading histories and testing conditions. *Acta Geotechnica*, 10, 131–155.
- Teng, T., & Wang, J. G. (2016). A thermally sensitive permeability model for coal-gas interactions including thermal fracturing and volatilization. *J Nat Gas Sci Eng*, 32, 319–333.
- Viete, D. R., & Ranjith, P. G. (2007). The mechanical behaviour of coal with respect to CO₂ sequestration in deep coal seams. *Fuel*, 86, 2667–2671.
- Wang, S., Elsworth, D., & Liu, J. (2011). Permeability evolution in fractured coal: The roles of fracture geometry and water-content. *International Journal of Coal Geology*, 87, 13–25.
- Wang, S. G., Elsworth, D., & Liu, J. S. (2013). Permeability evolution during progressive deformation of intact coal and implications for instability in underground coal seams. *International Journal of Rock Mechanics and Mining Sciences*, 58, 34–45.
- Wang, G., Liu, Z. Y., Wang, P. F., Guo, Y. Y., Wang, W. R., Huang, T. Y., et al. (2019a). The effect of gas migration on the deformation and permeability of coal under the condition of true triaxial stress. *Arabian Journal of Geosciences*, 12, 486.
- Wang, X., & Ma, L. W. (2019). Study on covering rough sets with topological methods. *CAAI Transactions on Intelligence Technology*, 4(3), 129–134.
- Wang, H. L., Xu, W. Y., & Zhu, F. (2014). The mechanical response of piles with consideration of pile-soil interactions under a periodic wave pressure. *Journal of Hydrodynamics*, 6, 921–929.
- Wang, R. Z., Yu, H. C., Wang, G. Z., Zhang, G. Q., & Wang, W. B. (2019b). Study on the dynamic and static characteristics of gas static thrust bearing with micro-hole restrictors. *International Journal of Hydromechanics*, 2(3), 189–202.
- Warren, J. E., & Root, P. J. (1963). The behavior of naturally fractured reservoirs. *SPE J*, 3, 245–255.
- Wasantha, P. L. P., Ranjith, P. G., & Shao, S. S. (2014). Energy monitoring and analysis during deformation of bedded-sandstone: Use of acoustic emission. *Ultrasonics*, 54(1), 217–226.
- Wold, M. B., Connell, L. D., & Choi, S. K. (2008). The role of spatial variability in coal seam parameters on gas outburst behaviour during coal mining. *International Journal of Coal Geology*, 75, 1–14.
- Wu, F., Gao, R., Zou, Q., Chen, J., Liu, W., & Peng, K. (2020). Long-term strength determination and nonlinear creep damage constitutive model of salt rock based on multi-stage creep test: Implications for underground natural gas storage in salt cavern. *Energy Science & Engineering*. <https://doi.org/10.1002/ese3.617>.
- Xie, H. P., Li, L. Y., Peng, R. D., & Ju, Y. (2009). Energy analysis and criteria for structural failure of rocks. *Journal of Rock Mechanics and Geotechnical Engineering*, 1(1), 11–20.
- Xie, G., Yin, Z., Wang, L., Hu, Z., & Zhu, C. (2017). Effects of gas pressure on the failure characteristics of coal. *Rock Mechanics and Rock Engineering*, 50, 1–13.
- Xin, C. P., Wang, K., Du, F., Zhang, X., Wang, G. D., & Liu, Y. L. (2018). Mechanical properties and permeability evolution of gas-bearing coal under phased variable speed loading and unloading. *Arabian Journal of Geosciences*, 11, 747.
- Yang, X. L., Cao, J., Cheng, X. Y., Liu, Y. H., Li, X. L., Sun, Z. G., et al. (2019a). Mechanical response characteristics and permeability evolution of coal samples under cyclic loading. *Energy Science and Engineering*, 7(5), 1588–1604.
- Yang, X. L., Wen, G. C., Dai, L. C., Sun, H. T., & Li, X. L. (2019b). Ground subsidence and surface cracks evolution from shallow-buried close-distance multi-seam mining: A case study in Bulianta Coal Mine. *Rock Mechanics Rock Engineering*, 52(8), 2835–2852.
- Yin, G. Z., Jiang, C. B., Wang, J. G., & Xu, J. (2013). Combined effect of stress, pore pressure and temperature on methane permeability in Anthracite Coal: An experimental study. *Transp Porous Med*, 100, 1–16.
- Yuan, L. (2016). Control of coal and gas outbursts in Huainan mines in China: A review. *J Rock Mech Geotech Eng*, 8, 559–567.
- Zhang, C., & Zhang, L. (2019). Permeability characteristics of broken coal and rock under cyclic loading and unloading. *Natural Resources Research*, 28, 1055–1069.
- Zhang, Q. G., Fan, X. Y., Liang, Y. C., Li, M. H., Li, G. Z., Ma, T. S., et al. (2017). Mechanical behavior and permeability evolution of reconstituted coal samples under various unloading confining pressures-implications for wellbore stability analysis. *Energies*, 10(3), 292.
- Zhang, Z. T., Zhang, R., Wu, S. Y., Deng, J. H., Zhang, Z. P., & Xie, J. (2019). The stress sensitivity and porosity sensitivity of coal permeability at different depths: A case study in the Pingdingshan Mining Area. *Rock Mechanics and Rock Engineering*, 52, 1539–1563.
- Zhao, Y., Cao, S. G., Li, Y., Yang, H. Y., Guo, P., Liu, G. J., et al. (2018). Experimental and numerical investigation on the effect of moisture on coal permeability. *Natural Hazards*, 90, 1201–1221.
- Zou, J. P., Chen, W. Z., Yang, D. S., Yu, H. D., & Yuan, J. Q. (2016). The impact of effective stress and gas slippage on coal permeability under cyclic loading. *Journal of Natural Gas Science and Engineering*, 31, 236–248.
- Zou, Q. L., & Lin, B. Q. (2018). Fluid-solid coupling characteristics of gas-bearing coal subject to hydraulic slotting: An experimental investigation. *Energy & Fuels*, 32, 1047–1060.
- Zou, Q. L., Liu, H., Cheng, Z. H., Zhang T. C., & Lin B. Q. (2019). Effect of slot inclination angle and borehole-slot ratio on mechanical property of pre-cracked coal: Implications for ECBM recovery using hydraulic slotting. *Natural Resources Research*. <https://doi.org/10.1007/s11053-019-09544-y>.
- Zou, Q. L., Liu, H., Zhang, Y. J., Li, Q. M., Fu, J. W., & Hu, Q. T. (2020). Rationality evaluation of production deployment of outburst-prone coal mines: A case study of nantong coal mine in Chongqing. *China. Safety Science*, 122, 104515.